JACS
JOURNAL OF THE AMERICAN CHEMICAL SOCIETY

Communication

Efficient Electrocatalytic Proton Reduction with Carbon Nanotube-Supported Metal-Organic Frameworks

Daniel Micheroni, Guangxu Lan, and Wenbin Lin

J. Am. Chem. Soc., **Just Accepted Manuscript** • DOI: 10.1021/jacs.8b09521 • Publication Date (Web): 03 Nov 2018

ACS Publications

is published by the American Chemical Society. 1155 Sixteenth Street N.W., Washington, DC 20036

Efficient Electrocatalytic Proton Reduction with Carbon Nanotube-Supported Metal-Organic Frameworks

Daniel Micheroni, Guangxu Lan, and Wenbin Lin*

Department of Chemistry, The University of Chicago, 929 East 57th Street, Chicago, Illinois 60637 United States

Supporting Information Placeholder

ABSTRACT: Hydrogen production from Earth-abundant catalysts remains an important but difficult challenge. Here we report the growth of Hf_{12}-porphyrin metal-organic frameworks (MOFs) on carbon nanotubes (CNTs) for electrocatalytic proton reduction. Covalent attachment of MOF nanoplates to conductive CNTs improves electron transfer from the electrode to Co-porphyrin active sites, leading to effective proton reduction via protonation of a Co^{I}-H intermediate. The Hf_{12}-CoDBP/CNT assembly afforded a turnover number of 32,000 in 30 minutes with a turnover frequency of 17.7 S^{-1}, placing it among the most active Co-based molecular electrocatalysts.

Growing global energy needs demand the development of renewable and clean energy technologies. Of numerous proposed approaches, hydrogen production via catalytic water splitting by either photochemical or electrochemical means presents an attractive solution due to the abundance of water and the ability of hydrogen to store energy and to transform inert molecules into chemical fuels.[1] However, most hydrogen is currently produced by steam reforming of natural gas as large-scale production of hydrogen using the solar energy input remains a technical challenge.

Hydrogen evolution reaction (HER) is a key half reaction of hydrogen production via water splitting. Typically, electrocatalytic HER is mediated by inorganic materials which fall near the top of the kinetic volcano plot based on the strength of the metal-hydrogen bond.[1, 2] However, these materials are often comprised of precious metals including Pt, Re, Ru, and Ir, making their large-scale implementation unrealistic.

To overcome the scarcity and high cost of precious metal electrocatalysts, numerous molecular systems and semiconductors have been developed based on Earth-abundant metals including Co,[3-5] Ni,[6-8] Fe,[9, 10] and Mo.[11-13] Tuning of organic ligands has afforded molecular HER catalysts with low overpotentials and high catalytic activities. However, these molecular HER catalysts are often insoluble in water and their activities are limited by diffusion to the electrodes.

As a new class of tunable molecular materials, metal-organic frameworks (MOFs) have provided a unique platform to design single-site solid catalysts.[14] The regularity of MOF structures affords high densities of catalytic sites, their high porosity allows for rapid mass transport, and their periodicity facilitates the characterization of catalytic centers. Although MOFs have been explored as photocatalysts for HER,[15-18] they have not found much use as electrocatalysts due to their electrically insulating nature and sluggish inter-ligand electron transfer. To improve electrical conductivity, MOFs were pyrolyzed to metal nanoparticles encapsulated in carbon matrices for electrocatalysis.[19-21] Alternatively, electrocatalysis was reported for ultra-thin films comprised of a few MOF layers dropcasted on or covalently tethered to the electrode surface.[22-30]

We recently reported a series of MOFs comprised of M_{12} (M = Zr and Hf) secondary building units (SBUs) and dicarboxylate ligands that fulfill many requirements of efficient electrocatalytsts.[31-33] These MOFs are a few nanometers thick with short inter-ligand distances (<1 nm), leading to efficient electron transfer through the MOF nanoplates. They are stable in aqueous environments. Herein we report the design of Hf_{12}-CoDBP comprised of Co-metalated 5,15-di(*p*-benzoato)-porphyrin (CoDBP) bridging ligands as a HER electrocatalyst (Figure 1). Molecular Co-porphyrin systems have previously been shown to effectively catalyze the HER.[21, 34, 35] Covalent tethering of Hf_{12}-CoDBP to multi-walled carbon nanotubes (CNTs) significantly improved electrical conductivity, leading to drastically enhanced HER turnover number (TON) and turnover frequency (TOF) for the Hf_{12}-CoDBP/CNT hybrid.

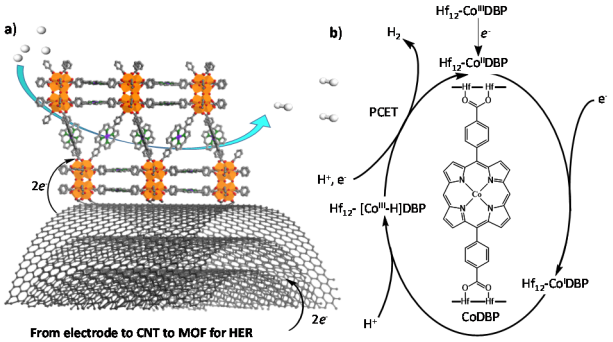

Figure 1. a) Covalent attachment of Hf_{12}-CoDBP to CNTs enhances electrocatalytic HER at CoDBP centers. b) The HER is proposed to proceed through a Co^{III}-H intermediate. Orange = Hf, purple = Co, black = C, red= O, green = N, and white = H.

Hf_{12}-CoDBP with the ideal composition of $Hf_{12}O_8(\mu_3\text{-}OH)_8(\mu_2\text{-}OH)_6(CoDBP)_9$ was prepared via a solvothermal reaction between H_2(CoDBP) and $HfCl_4$ in DMF at 85 °C for 72h. Alternatively, Hf_{12}-CoDBP was prepared by metalation of known Hf_{12}-H_2DBP with $CoCl_2$ in DMF at 80 °C.[36] Both procedures afforded the same MOF structure with four major PXRD peaks at 2θ = 3.8, 6.55, 7.57, and 9.99 ° corresponding to hko

indices; other PXRD peaks are unobservable due to inherent defects along the *c*-direction.[33] Hf_{12}-CoDBP has a diameter of 30-100 nm (Figures 2 and S1) by TEM and a thickness ranging of 10-40 nm by atomic force microscopy (AFM), correlating to the stacking of 3 to 12 unit cells along the c-axis (Figure 2a). The thickness of Hf_{12}-CoDBP is thus smaller than that of the electric double layer, making it a potential candidate for electrocatalysis.

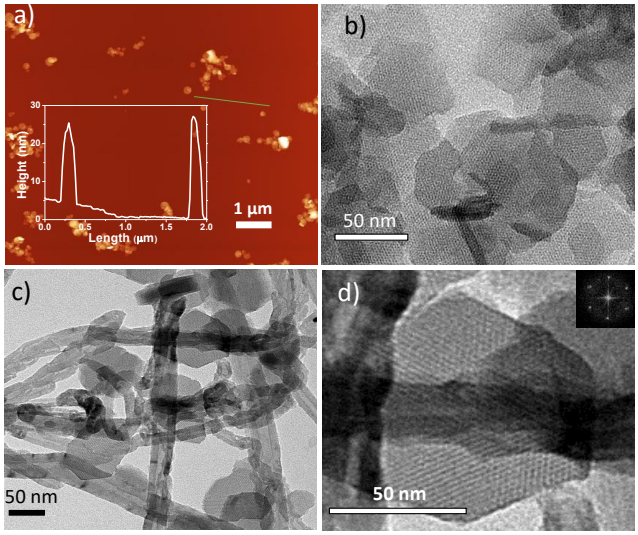

Figure 2. a) AFM analysis of Hf_{12}-CoDBP shows 20 and 25 nm thick nanoplates. b-d) TEM images of Hf_{12}-CoDBP (b) and Hf_{12}-CoDBP/CNT (c, d) show the retention of crystalline MOF nanoplate morphology when covalently bound to CNTs. The Fast Fourier Transform in inset of (d) shows expected 6-fold symmetry along the c-axis.

Hf_{12}-CoDBP/CNT was synthesized by heating a DMF solution of CoDBP and $HfCl_4$ in the presence of carboxylated multi-walled CNTs at 85 °C for 72 h. The carboxylate groups on the CNTs allow for direct attachment to the MOF via the SBU, affording a densely packed Hf_{12}-CoDBP/CNT heterostructure with the unchanged plate-like morphology of Hf_{12}-CoDBP (Figure 2c, d). PXRD studies indicated that Hf_{12}-CoDBP/CNT adopts the same crystalline structure as Hf_{12}-CoDBP (Figure S3), while high resolution TEM (HRTEM) images showed lattice points with inter-SBU distances of 2.7 nm. The Fast Fourier Transform (FFT) showed six-fold symmetry which is consistent with the projection of Hf-CoDBP structure along the (001) direction (Figure 2d).

X-ray photoelectron spectroscopy (XPS) indicated the presence of Co^{3+} and Hf^{4+} centers in Hf_{12}-CoDBP/CNT (Figure S4). Integration of XPS $Co2P_{3/2}$ and $Hf4d_{3/2}$ peaks gave a Hf:Co ratio of 1.78 for Hf_{12}-DBP-Co/CNT. Thermogravimetric analysis (TGA) gave a Hf:porphyrin ratio of 1.46 - 1.66 (Figure S5) and inductively coupled plasma-mass spectrometry (ICP-MS) gave a Hf:Co ratio of 1.57:1 for Hf_{12}-DBP-Co/CNT. The Hf:CoDBP ratios from these analyses gave an average Hf:CoDBP ratio of 1.62, which deviates from 1.33 expected for the idealized Hf_{12}-CoDBP structure. The MOF structure of Hf_{12}-CoDBP/CNT is thus highly defected along the c-axis and has an empirical formula of $Hf_{12}O_8(\mu_3\text{-}OH)_8(\mu_2\text{-}OH)_6(CoDBP)_{7.4}$. Minimal Co^{3+} ions leached from CoDBP during the MOF growth as shown by UV-Vis spectroscopy (Figures S6 and S7).

Nitrogen sorption studies revealed a Brunauer-Emmett-Teller (BET) surface area of 115.4 4 m^2/g for Hf_{12}-CoDBP/CNT, which is significantly higher than that of CNTs (S_{BET} = 78.12 m^2/g, Figure S8), due to the deposition of highly porous Hf_{12}-CoDBP (S_{BET} = 509.3 m^2/g) on CNTs. The pore sizes of Hf_{12}-CoDBP/CNT ranged from 2 to 3 nm for the MOF lattice and 4 to 10 nm for the natural porosity of the CNTs. S_{BET} and TGA results thus suggest that Hf_{12}-CoDBP comprises 20-25 % of the overall mass of Hf_{12}-CoDBP/CNT. The high loading of Hf_{12}-CoDBP is also evident in TEM images.

The structural and chemical properties of Hf_{12}-CoDBP lend itself toward electrochemical applications when covalently attached to CNTs. Direct tethering of Hf_{12}-CoDBP to a conductive surface increases the rate of electron transfer to CoDBP catalytic sites. The nanoplate morphology of Hf_{12}-CoDBP places active sites in close proximity to the conductive support, the electrolyte, and the substrate simultaneously. These features not only overcome the diffusion constraint of the active catalyst, but also prevent detrimental bimolecular deactivation pathways as a result of active site isolation. The deposition of highly porous Hf_{12}-CoDBP on CNTs also increases the number of active sites on the electrode surface.

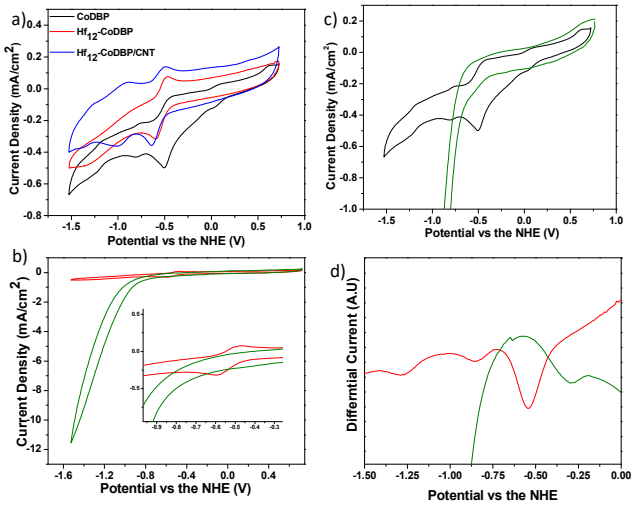

Figure 3. a) The CV curves of the homogenous species (black), Hf_{12}-CoDBP (Red), and Hf_{12}-CoDBP/CNT (Blue) in 0.1 M $[TBA]PF_6$ dissolved in acetonitrile. b,c) The CV curves of H_2(CoDBP) (b) and Hf12-CoDBP (c) with (blue) and without (red) TFA (0.026 M) show similar hydrogen production behavior. d) Differential pulse voltammetry of Hf_{12}-CoDBP in acetonitrile with (blue) and without (red) TFA suggest the HER process occurs via protonation of a Co^{I}-H intermediate.

Cyclic voltammetry measurements of Hf_{12}-CoDBP, Hf_{12}-CoDBP/CNT, and homogenous CoDBP showed a reversible one electron peak at -0.485 V vs the NHE in acetonitrile for the $Co^{II/I}$ reduction of CoDBP (Figure 3).[37] Upon addition of 0.026 M trifluoroacetic acid (TFA) as a proton source, the $Co^{I/II}$ anodic peak disappeared with a concurrent increase in current density attributable to catalytic proton reduction. The similar behavior seen in Hf_{12}-CoDBP, Hf_{12}-CoDBP/CNT, and CoDBP indicates an identical catalytic process, likely through the Heyrovsky pathway via a Co^{I}-H intermediate, as the physical constraints of the MOF and the thermodynamics of the system ensure the process proceeds via the unimolecular pathway through protonation to a Co^{I} species.

Integration of the Co^{II}/Co^{I} anodic peak for the Hf_{12}-CoDBP/CNT species in acetonitrile revealed that 31.9% of total Co species (0.947 nmol by ICP-MS) on the electrode surface were electrochemically active. This value represents a 114 times increase over that of Hf_{12}-CoDBP; dropcasting 0.1 mg of Hf_{12}-CoDBP/CNT on a 0.0625 cm^2 glassy carbon electrode yields a catalytically active surface area of 49.6 cm^2 (Figure S10). A linear relationship for the log of the current vs the log of the scan rate with a slope of 0.54 was found for Hf_{12}-CoDBP/CNT, indicating the redox process occurs via a charge hopping mechanism (Figure S11). In comparison, Hf_{12}-CoDBP synthesized with non-carboxylated CNTs showed only 0.29% electrochemically active Co sites (Figure S12d). These results demonstrate the importance of covalent tethering of the MOF to the CNT in achieving good electrocatalytic activity by increasing the overall surface area of the electrode to enhance electron injection into the catalytic sites.

Hf_{12}-CoDBP/CNT greatly outperformed Hf_{12}-CoDBP and Hf_{12}-CoDBP/non-carboxylated CNT in electrocatalytic HER in aqueous media (Table S2). Dropcasted Hf_{12}-CoDBP/CNT exhibited a remarkable electrocatalytic HER activity in a pH = 1 perchloric acid solution, with a current density of 10 mA/cm^2 at an overpotential (η) of 650 mV. This corresponds to a Tafel slope of 178 mV/dec, which is consistent with a rate limiting step involving the adsorption of a proton to the catalytic site within the Volmer portion of the HER (Figure 4a,b). The importance of the CNT tethering was further supported by the increased current densities, TONs, and Faradaic efficiencies for Hf_{12}-CoDBP/CNT samples with higher CNT loadings (Figure S13). However, long term stability of the Hf_{12}-CoDBP/CNT system remained an issue as stirring and hydrogen bubble formation tended to shear the catalyst off the electrode surface.

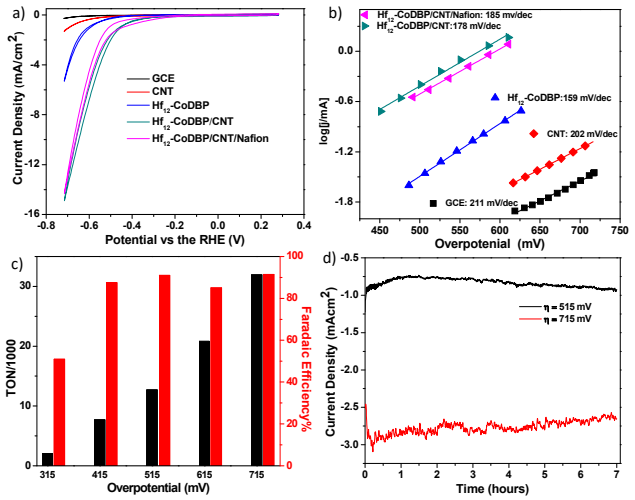

Figure 4. a) CV curves of Hf_{12}-CoDBP/CNT and Hf_{12}-CoDBP/CNT/Nafion compared to their controls in 0.1 M aqueous perchloric acid and b) their corresponding Tafel curves. c) TON (black) and Faradaic efficiency (red) measurements of Hf_{12}-CoDBP/CNT/Nafion after 30 minutes of electrolysis at varying overpotenials at pH = 1. d) Time-dependent current densities of Hf_{12}-CoDBP/CNT/Nafion at η = 515 and 715 mV, showing sustained HER for >7 hours.

Proton conducting Nafion was added to the Hf_{12}-CoDBP/CNT suspension to improve thin film stability. Hf_{12}-CoDBP/CNT/Nafion maintained stable currents for varying time lengths of electrolysis at a η of 715 mV, producing hydrogen with a TON of 3.2×10^4 after thirty minutes of electrolysis and a TOF= 17.7 s^{-1} (Figure 3c). Hydrogen gas was detected at a η of 315 mV at pH = 1 and Hf_{12}-CoDBP/CNT/Nafion showed moderate activity in aqueous solutions up to pH = 5 (Figure S15). In comparison, bare glassy carbon electrode, bare CNTs, and Hf_{12}-H_2DBP/CNT need an overpotential of ⩾515 mV to detect any trace of hydrogen, most likely from nanoparticle formation [38, 39] at a rate that is at least one order of magnitude lower than that of Hf_{12}-CoDBP/CNT/Nafion (Table S1).

Hf_{12}-CoDBP/CNT/Nafion showed good efficacy of electrocatalytic HER at varying potentials (Figure 4c). At η > 415 mV, the Faradaic efficiency averaged at 92.4%. The Faradaic efficiency was only 51.2% at η = 315 mV, likely due to dominance of CNT reduction and other side reactions over HER at low overpotentials. Above η > 415, the TON showed a roughly linear increase with ovepotential; a slight tailing off was observed at higher potentials indicative of saturation of active sites with protons. Hf_{12}-CoDBP/CNT/Nafion also showed very good stability with consistent hydrogen production across varying potentials for at least seven hours (Figure 3d). Hf_{12}-CoDBP/CNT is thus competitive with other water stable porphyrin and Co HER catalysts in terms of onset potential and TON (Table S3).

In addition to enhancing stability, Nafion also slows down the transport of larger ions (such as Co^{2+}) to the electrode surface to mitigate the formation of nanoparticles, which can also catalyze proton reduction, thus ensuring that HER by Hf_{12}-CoDBP/CNT is entirely molecular in nature. In agreement with this conjecture, Hf_{12}-CoDBP/CNT/Nafion showed good stability upon 10000 CV cycles and no significant change in the CV curve before and after electrocatalytic HER (Figure S17). In addition, ICP-MS analyses showed negligible leaching of Co (<0.2%) and Hf (<0.1 %) from Hf_{12}-CoDBP/CNT/Nafion after electrolysis at η=715 mV for one hour based on the metal loadings on the electrode surface. PXRD patterns (Figure S3) and UV-Vis spectra (Figure S17c) of Hf_{12}-CoDBP/CNT/Nafion remained unchanged after electrolysis at η=715 mV for 18 hours. TEM imaging showed no Co nanoparticle formation during electrolysis (Figure S17d).

In conclusion, we have synthesized Co-porphyrin MOFs supported on CNT for efficient electrocatalytic proton reduction. Covalent attachment of Co-porphyrin MOFs to CNTs significantly increases the number of catalytically active sites by increasing both the surface areas of conductive supports and the percentage of active sites. The MOF/CNT hybrid is highly active for HER in acidic media with an onset potential of 315 mV and TOFs of over 17.7 s^{-1}. This straightforward synthetic strategy should be amenable to the design of other MOF/CNT heterostructures for electrochemical applications.

ASSOCIATED CONTENT

Supporting Information

The Supporting Information is available free of charge via the Internet at http://pubs.acs.org. Synthesis and characterization of MOF and MOF/CNT samples, cyclic voltammetry, and electrocatalytic proton reduction.

AUTHOR INFORMATION

Corresponding Author

*wenbinlin@uchicago.edu

Notes

The authors declare no competing financial interests.

ACKNOWLEDGMENT

This work was partially supported by National Science Foundation (DMR-1308229).

REFERENCES

(1) Trasatti, S., Work function, electronegativity, and electrochemical behavior of metals. III. Electrolytic hydrogen evolution in acid solutions. *J. Electroanal. Chem. Interfacial Electrochem.* **1972,** *39* (1), 163-84.

(2) Norskov, J. K.; Bligaard, T.; Logadottir, A.; Kitchin, J. R.; Chen, J. G.; Pandelov, S.; Stimming, U., Trends in the exchange current for hydrogen evolution. *J. Electrochem. Soc.* **2005,** *152* (3), J23-J26.

(3) Hu, X. L.; Brunschwig, B. S.; Peters, J. C., Electrocatalytic Hydrogen Evolution at Low Overpotentials by Cobalt Macrocyclic Glyoxime and Tetraimine Complexes. *J. Am. Chem. Soc.* **2007,** *129* (29), 8988-8998.

(4) Sun, Y.; Bigi, J. P.; Piro, N. A.; Tang, M. L.; Long, J. R.; Chang, C. J., Molecular Cobalt Pentapyridine Catalysts for Generating Hydrogen from Water. *J. Am. Chem. Soc.* **2011,** *133* (24), 9212-9215.

(5) Dempsey, J. L.; Brunschwig, B. S.; Winkler, J. R.; Gray, H. B., Hydrogen Evolution Catalyzed by Cobaloximes. *Acc. Chem. Res.* **2009,** *42* (12), 1995-2004.

(6) Tsay, C.; Yang Jenny, Y., Electrocatalytic Hydrogen Evolution under Acidic Aqueous Conditions and Mechanistic Studies of a Highly Stable Molecular Catalyst. *J Am Chem Soc* **2016,** *138* (43), 14174-14177.

(7) Bianchini, C.; Fornasiero, P., A Synthetic Nickel Electrocatalyst with a Turnover Frequency above 100 000 s-1 for H2 Production. *ChemCatChem* **2012,** *4* (1), 45-46.

(8) Wilson Aaron, D.; Shoemaker, R. K.; Miedaner, A.; Muckerman, J. T.; DuBois Daniel, L.; DuBois, M. R., Nature of hydrogen interactions with Ni(II) complexes containing cyclic phosphine ligands with pendant nitrogen bases. *Proc Natl Acad Sci U S A* **2007,** *104* (17), 6951-6.

(9) Kaur-Ghumaan, S.; Schwartz, L.; Lomoth, R.; Stein, M.; Ott, S., Catalytic Hydrogen Evolution from Mononuclear Iron(II) Carbonyl Complexes as Minimal Functional Models of the [FeFe] Hydrogenase Active Site. *Angew. Chem., Int. Ed.* **2010,** *49* (43), 8033-8036, S8033/1-S8033/12.

(10) Gloaguen, F.; Rauchfuss, T. B., Small molecule mimics of hydrogenases: hydrides and redox. *Chem. Soc. Rev.* **2009,** *38* (1), 100-108.

(11) Benck, J. D.; Hellstern, T. R.; Kibsgaard, J.; Chakthranont, P.; Jaramillo, T. F., Catalyzing the Hydrogen Evolution Reaction (HER) with Molybdenum Sulfide Nanomaterials. *ACS Catal.* **2014,** *4* (11), 3957-3971.

(12) Vrubel, H.; Hu, X., Molybdenum Boride and Carbide Catalyze Hydrogen Evolution in both Acidic and Basic Solutions. *Angew. Chem., Int. Ed.* **2012,** *51* (51), 12703-12706.

(13) Xing, Z.; Liu, Q.; Asiri, A. M.; Sun, X., Closely interconnected network of molybdenum phosphide nanoparticles: a highly efficient electrocatalyst for generating hydrogen from water. *Adv. Mater. (Weinheim, Ger.)* **2014,** *26* (32), 5702-5707.

(14) Drake, T.; Ji, P.; Lin, W., Site Isolation in Metal-Organic Frameworks Enables Novel Transition Metal Catalysis. *Acc. Chem. Res.* **2018**, Ahead of Print.

(15) Horiuchi, Y.; Toyao, T.; Saito, M.; Mochizuki, K.; Iwata, M.; Higashimura, H.; Anpo, M.; Matsuoka, M., Visible-Light-Promoted Photocatalytic Hydrogen Production by Using an Amino-Functionalized Ti(IV) Metal-Organic Framework. *J. Phys. Chem. C* **2012,** *116* (39), 20848-20853.

(16) Fateeva, A.; Chater, P. A.; Ireland, C. P.; Tahir, A. A.; Khimyak, Y. Z.; Wiper, P. V.; Darwent, J. R.; Rosseinsky, M. J., A Water-Stable Porphyrin-Based Metal-Organic Framework Active for Visible-Light Photocatalysis. *Angew. Chem., Int. Ed.* **2012,** *51* (30), 7440-7444, S7440/1-S7440/17.

(17) Wu, P.; Jiang, M.; Li, Y.; Liu, Y.; Wang, J., Highly efficient photocatalytic hydrogen production from pure water via a photoactive metal-organic framework and its PDMS@MOF. *J. Mater. Chem. A* **2017,** *5* (17), 7833-7838.

(18) Lan, G.; Zhu, Y.-Y.; Veroneau, S. S.; Xu, Z.; Micheroni, D.; Lin, W., Electron Injection from Photoexcited Metal-Organic Framework Ligands to Ru2 Secondary Building Units for Visible-Light-Driven Hydrogen Evolution. *J. Am. Chem. Soc.* **2018,** *140* (16), 5326-5329.

(19) deKrafft, K. E.; Wang, C.; Lin, W., Metal-Organic Framework Templated Synthesis of Fe2O3/TiO2 Nanocomposite for Hydrogen Production. *Adv. Mater. (Weinheim, Ger.)* **2012,** *24* (15), 2014-2018.

(20) Zhang, J.; An, B.; Hong, Y.; Meng, Y.; Hu, X.; Wang, C.; Lin, J.; Lin, W.; Wang, Y., Pyrolysis of metal-organic frameworks to hierarchical porous Cu/Zn-nanoparticle@carbon materials for efficient CO2 hydrogenation. *Mater. Chem. Front.* **2017,** *1* (11), 2405-2409.

(21) Xia, B. Y.; Yan, Y.; Li, N.; Wu, H. B.; Lou, X. W.; Wang, X., A metal-organic framework-derived bifunctional oxygen electrocatalyst. *Nat. Energy* **2016,** *1* (1), 15006.

(22) Kornienko, N.; Zhao, Y.; Kley, C. S.; Zhu, C.; Kim, D.; Lin, S.; Chang, C. J.; Yaghi, O. M.; Yang, P., Metal-Organic Frameworks for Electrocatalytic Reduction of Carbon Dioxide. *J. Am. Chem. Soc.* **2015,** *137* (44), 14129-14135.

(23) Lu, X.-F.; Liao, P.-Q.; Wang, J.-W.; Wu, J.-X.; Chen, X.-W.; He, C.-T.; Zhang, J.-P.; Li, G.-R.; Chen, X.-M., An Alkaline-Stable, Metal Hydroxide Mimicking Metal-Organic Framework for Efficient Electrocatalytic Oxygen Evolution. *J. Am. Chem. Soc.* **2016,** *138* (27), 8336-8339.

(24) Wurster, B.; Grumelli, D.; Hoetger, D.; Gutzler, R.; Kern, K., Driving the Oxygen Evolution Reaction by Nonlinear Cooperativity in Bimetallic Coordination Catalysts. *J. Am. Chem. Soc.* **2016,** *138* (11), 3623-3626.

(25) Miner, E. M.; Gul, S.; Ricke, N. D.; Pastor, E.; Yano, J.; Yachandra, V. K.; Van Voorhis, T.; Dinca, M., Mechanistic Evidence for Ligand-Centered Electrocatalytic Oxygen Reduction with the Conductive MOF Ni3(hexaiminotriphenylene)2. *ACS Catal.* **2017,** *7* (11), 7726-7731.

(26) Hod, I.; Deria, P.; Bury, W.; Mondloch, J. E.; Kung, C.-W.; So, M.; Sampson, M. D.; Peters, A. W.; Kubiak, C. P.; Farha, O. K.; Hupp, J. T., A porous proton-relaying metal-organic framework material that accelerates electrochemical hydrogen evolution. *Nat. Commun.* **2015,** *6*, 8304.

(27) Hod, I.; Sampson, M. D.; Deria, P.; Kubiak, C. P.; Farha, O. K.; Hupp, J. T., Fe-Porphyrin-Based Metal–Organic

Framework Films as High-Surface Concentration, Heterogeneous Catalysts for Electrochemical Reduction of CO2. *ACS Catal.* **2015,** *5* (11), 6302-6309.

(28) Usov, P. M.; Huffman, B.; Epley, C. C.; Kessinger, M. C.; Zhu, J.; Maza, W. A.; Morris, A. J., Study of Electrocatalytic Properties of Metal–Organic Framework PCN-223 for the Oxygen Reduction Reaction. *ACS Applied Materials & Interfaces* **2017,** *9* (39), 33539-33543.

(29) Miner, E. M.; Wang, L.; Dinca, M., Modular O_2 electroreduction activity in triphenylene-based metal-organic frameworks. *Chem. Sci.* **2018,** *9* (29), 6286-6291.

(30) Lin, S.; Pineda-Galvan, Y.; Maza, W. A.; Epley, C. C.; Zhu, J.; Kessinger, M. C.; Pushkar, Y.; Morris, A. J., Electrochemical Water Oxidation by a Catalyst-Modified Metal-Organic Framework Thin Film. *ChemSusChem* **2017,** *10* (3), 469.

(31) Ji, P.; Manna, K.; Lin, Z.; Feng, X.; Urban, A.; Song, Y.; Lin, W., Single-Site Cobalt Catalysts at New Zr12(μ3-O)8(μ3-OH)8(μ2-OH)6 Metal-Organic Framework Nodes for Highly Active Hydrogenation of Nitroarenes, Nitriles, and Isocyanides. *J. Am. Chem. Soc.* **2017,** *139* (20), 7004-7011.

(32) Ni, K.; Lan, G.; Chan, C.; Quigley, B.; Lu, K.; Aung, T.; Guo, N.; La Riviere, P.; Weichselbaum, R. R.; Lin, W., Nanoscale metal-organic frameworks enhance radiotherapy to potentiate checkpoint blockade immunotherapy. *Nat. Commun.* **2018,** *9* (1), 1-12.

(33) Lu, K.; He, C.; Guo, N.; Chan, C.; Ni, K.; Lan, G.; Tang, H.; Pelizzari, C.; Fu, Y.-X.; Spiotto, M. T.; Weichselbaum, R. R.; Lin, W., Low-dose X-ray radiotherapy–radiodynamic therapy via nanoscale metal–organic frameworks enhances checkpoint blockade immunotherapy. *Nat. Biomed. Eng.* **2018**.

(34) Beyene, B. B.; Mane, S. B.; Hung, C.-H., Highly efficient electrocatalytic hydrogen evolution from neutral aqueous solution by a water-soluble anionic cobalt(II) porphyrin. *Chem. Commun. (Cambridge, U. K.)* **2015,** *51* (81), 15067-15070.

(35) Kellett, R. M.; Spiro, T. G., Cobalt porphyrin electrode films as hydrogen catalysts. *Inorg. Chem.* **1985,** *24* (15), 2378-82.

(36) Hu, B.; Sun, C.; Deng, Q.; Liu, Z., Synthesis and catalytic properties of a series of cobalt porphyrins as cytochrome P450 model: the effect of substituents on the catalytic activity. *J. Inclusion Phenom. Macrocyclic Chem.* **2013,** *76* (3-4), 345-352.

(37) Walker, F. A.; Beroiz, D.; Kadish, K. M., Electronic effects in transition metal porphyrins. 2. The sensitivity of redox and ligand addition reactions in para-substituted tetraphenylporphyrin complexes of cobalt(II). *J. Am. Chem. Soc.* **1976,** *98* (12), 3484-9.

(38) Zhou, W.; Zhou, J.; Zhou, Y.; Lu, J.; Zhou, K.; Yang, L.; Tang, Z.; Li, L.; Chen, S., N-Doped Carbon-Wrapped Cobalt Nanoparticles on N-Doped Graphene Nanosheets for High-Efficiency Hydrogen Production. *Chem. Mater.* **2015,** *27* (6), 2026-2032.

(39) (Zou, X.; Huang, X.; Goswami, A.; Silva, R.; Sathe, B. R.; Mikmekova, E.; Asefa, T., Cobalt-Embedded Nitrogen-Rich Carbon Nanotubes Efficiently Catalyze Hydrogen Evolution Reaction at All pH Values. *Angew. Chem., Int. Ed.* **2014,** *53* (17), 4372-4376.

TOC Graphic